PCCP

PAPER

View Article Online
View Journal | View Issue

Cite this: *Phys. Chem. Chem. Phys.*, 2015, **17**, 398

Plasma-induced grafting of polyacrylamide on graphene oxide nanosheets for simultaneous removal of radionuclides†

Wencheng Song,[ab] Xiangxue Wang,[b] Qi Wang,[b] Dadong Shao[b] and Xiangke Wang*[acd]

Received 24th September 2014,
Accepted 30th October 2014

DOI: 10.1039/c4cp04289a

www.rsc.org/pccp

Polyacrylamide (PAM) grafted graphene oxide (denoted as PAM/GO) was synthesized by the plasma-induced polymerization technique and applied as an adsorbent for the simultaneous removal of radionuclides from radioactive wastewater. The interactions of PAM/GO with the radionuclides U(VI), Eu(III) and Co(II) were studied, along with their sorption kinetics. The results indicated that radionuclide sorption on PAM/GO was affected by the solution pH and ionic strength. The maximum sorption capacities of U(VI), Eu(III) and Co(II) on PAM/GO (0.698, 1.245 and 1.621 mmol g^{-1}, respectively) at pH = 5.0 ± 0.1 and T = 295 K were much higher than those of radionuclides on GO and other adsorbents. The thermodynamic data (ΔH^0, ΔS^0 and ΔG^0) calculated from the temperature-dependent sorption isotherms suggested that the sorption of radionuclides on PAM/GO was a spontaneous and endothermic process. These results indicate that PAM/GO is a promising material for the control of radionuclide pollution.

Introduction

Radionuclide pollution has aroused considerable concerns due to the application of nuclear weapons, utilization of nuclear energy, and uranium mining.[1] The presence of radioactive nuclides and fission products, even at very low doses, is an issue of great concern because they can pose a serious threat to human beings. Recently, synthetic adsorbents, including resins,[2] nano-porous materials,[3] carbon nanotubes,[4] and graphene[5] have been demonstrated to remove radionuclides efficiently. These reports mainly investigated how radionuclide adsorption onto adsorbents was affected by environmental factors such as temperature and contact time. Nevertheless, low adsorbabilities limited these materials' applicability in the management of radioactive wastewater.

Graphene has a large specific surface area (about 2620 $m^2\ g^{-1}$),[6] which facilitates its potential application in environmental pollution control and remediation.[5,7] Graphene oxide (GO), one of the important graphene derivatives, has many oxygen-containing functional groups on its basal plane and on the edges of its sheets in the form of epoxy, hydroxyl, and carboxyl groups.[8] These oxygen-containing groups can bind metal ions[9] and organic pollutants[10] through coordination, electrostatic interaction and/or hydrogen bonding *etc.*, which ensures its potential application in environmental pollution control and remediation. However, GO has a tendency to form aggregates because of its strong interplanar interactions. As a result, a considerable part of its surface area will be lost,[11] limiting its practical application in wastewater treatment. In order to reduce and to overcome the above disadvantages, a variety of polymers have been grafted onto the surface of GO to prevent its aggregation and to enhance its sorption capacity.[12] Polyacrylamide (PAM), in which the amide groups are used as the active sites to enrich metal ions and to form stable metal ion-amide linkages between amide groups and metal ions, is widely applied in wastewater treatment.[13] However, previous studies have focused on single-component removal,[12,13] studies on the simultaneous removal of radionuclides from radioactive wastewater are still not available.

In the present study, we synthesized PAM/GO nanosheets by the plasma-induced polymerization technique,[14] and applied them as an adsorbent to simultaneously remove U(VI), Eu(III) and Co(II) ions from radioactive wastewater. The as-prepared PAM/GO was characterized using scanning electron microscopy (SEM), transmission electron microscopy (TEM), Fourier transformed infrared spectroscopy (FT-IR), thermo gravimetric analysis (TGA), Raman spectroscopy and potentiometric acid–base titrations. The PAM/GO nanosheets were applied to adsorb U(VI), Eu(III)

[a] *School of Environment and Chemical Engineering, North China Electric Power University, Beijing 102206, P. R. China. E-mail: xkwang@ipp.ac.cn, xkwang@ncepu.edu.cn; Fax: +86-551-65591310; Tel: +86-551-65592788*
[b] *Institute of Plasma Physics, Chinese Academy of Sciences, P.O. Box 1126, 230031, Hefei, China*
[c] *Faculty of Engineering, King Abdulaziz University, Jeddah 21589, Saudi Arabia*
[d] *Collaborative Innovation Center of Radiation Medicine of Jiangsu Higher Education Institutions, P. R. China*

† Electronic supplementary information (ESI) available. See DOI: 10.1039/c4cp04289a

and Co(II) from radioactive wastewater to evaluate the application of PAM/GO in radionuclide pollution control. In addition, the possible adsorption mechanism was discussed.

Experimental section

Preparation of GO

GO was prepared by a modified Hummers method from flake graphite.[15] Briefly, under mechanical stirring and ice-water bath conditions, 1.0 g graphite, 1.0 g $NaNO_3$, and 40 mL H_2SO_4 were mixed in an Erlenmeyer flask, and then 6.0 g $KMnO_4$ was slowly added. The mixture reacted at 20 ± 1 °C for 5 days. Later, 85 mL Milli-Q water was added into the mixture. The solution was stirred for 30 min at 90 ± 1 °C, and then cooled to 60 °C. 6 mL H_2O_2 (30%) was added slowly to remove the residual $KMnO_4$. The solution was filtered and rinsed with Milli-Q water thoroughly. The filter cake was vacuum dried and a dark brown GO powder was obtained.

Preparation of PAM/GO

The synthesis of PAM/GO was carried out in a dielectric barrier discharge (DBD) plasma reactor at ambient pressure.[16] A 30 mg sample of the resulting GO powder was dispersed in 30 mL Milli-Q water by sonication for 1.5 h, and a stable GO solution was formed. To prepare PAM/GO nanosheets, 0.1 g acrylamide was dissolved in 20 mL Milli-Q water and the solution was added into the aqueous GO solution under mild stirring. After the suspension was purged with argon for 30 min, DBD plasma treatment was initiated with a voltage of 120 V and power of 240 W at room temperature for 30 min (detailed information is listed in the ESI†).

Sorption of radionuclides on PAM/GO and GO

The sorption of radionuclides on PAM/GO was investigated using the batch technique. Specific amounts of PAM/GO suspension and NaCl solution were mixed in 10 mL polyethylene centrifuge tubes. After that, radionuclide solution was added to achieve the desired concentrations of different components, and the pH was adjusted to the desired values with dilute HCl or NaOH. The suspensions were shaken for 24 h to achieve sorption equilibrium and then centrifuged at 9000 rpm for 15 min. The concentrations of U(VI) and Co(II) were determined using inductively coupled plasma atomic emission spectroscopy (ICP-AES) (ICP 300, Thermo Fisher Scientific, USA), and the radionuclide $^{152+154}$Eu(III) concentration was analyzed using liquid scintillation counting (Packard 3100 TR/AB Liquid Scintillation analyzer, Perkin-Elmer) with a scintillation cocktail (ULTIMA GOLD ABTM, Packard). The amount of radionuclides adsorbed on PAM/GO or GO was calculated from the difference between the initial concentration and the final one (sorption % = $(C_0 - C_e) \times 100\%/C_0$ and $K_d = (C_0 - C_e) - V/(C_e \times m)$, where K_d is the distribution coefficient, m (g) is the mass of PAM/GO or GO, and V (L) is the volume of the suspension). All tests were conducted in duplicate.

Results and discussion

Characterization

The morphology and microstructure of GO and PAM/GO were characterized using SEM and TEM images. As can be seen from Fig. 1a, the GO nanosheets are found to stack together, while the PAM/GO nanosheets are well dispersed (Fig. 1b). Fig. 1c shows the TEM image of GO, in which bare GO surfaces and aggregated GO are observed. However, as seen from the TEM image of the PAM/GO nanosheets (Fig. 1d), there are many dark dots on the GO nanosheets, which are proven to be nanosized PAM domains chemically grafted on the GO surface from the results of FT-IR, Raman, XRD analysis in the following section. These data suggest that PAM was successfully grafted on the GO surfaces. The N_2–BET specific surface area of PAM/GO (92.1 $m^2\ g^{-1}$) is larger than that of GO (60.8 $m^2\ g^{-1}$), which also supports the result (see Fig. S1, ESI†).

Fig. 2a shows the FT-IR spectra of the GO and PAM/GO nanosheets. The absorption bands before grafting with PAM at 1221, 1620, 1721, and 3450 cm^{-1} correspond to C–O bonds, sp^2 C=C bonds, C=O stretching vibrations, and –OH stretching vibrations.[5c,17] After grafting with PAM, the FT-IR spectrum of the PAM/GO nanosheets presents similar characteristic peaks related to the C=O (1686 cm^{-1}), C–O (1190 cm^{-1}) and –OH stretching vibrations, which can be observed to have shifted little after modification with PAM. Furthermore, it is easy to note that there are additional characteristic peaks, such as the double peaks occurring at 1320 and 1349 cm^{-1} (stretching vibration of –NH groups), 1413 and 1453 cm^{-1} (deformation vibration of –NH groups), and the typical C–H vibration at 2930 cm^{-1}. These characteristic peaks are in agreement with the infrared spectrum of polyacrylamide,[18] which confirms that PAM has been successfully grafted on GO.

The TGA technique was used to evaluate the weight percentage of PAM in PAM/GO (Fig. 2b). The mass loss below 100 °C was considered to be the weight loss from moisture evaporation.

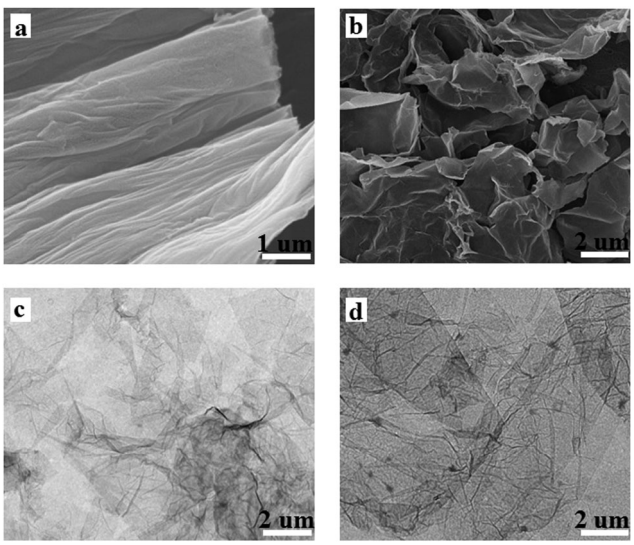

Fig. 1 SEM images of GO (a) and PAM/GO (b); TEM images of GO (c) and PAM/GO (d).

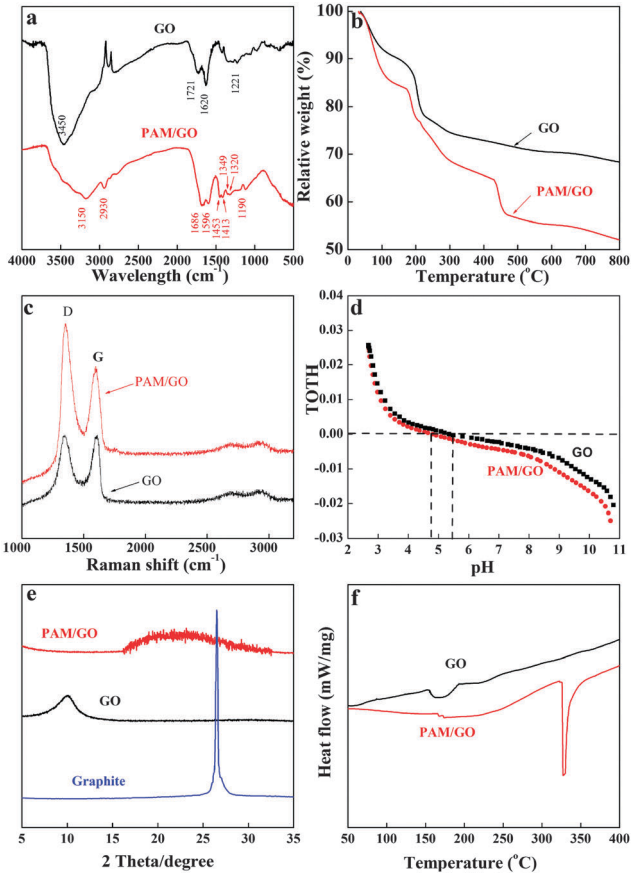

Fig. 2 FT-IR spectra of GO and PAM/GO (a); TGA curves of GO and PAM/GO (b); Raman spectra of GO and PAM/GO (c); potentiometric acid–base titrations of GO and PAM/GO (d); XRD patterns of natural graphite, GO and PAM/GO (e); DSC curves of GO and PAM/GO (f).

The mass loss between 150 and 250 °C was presumably attributed to the decomposition of some oxygen-containing functional groups.[19] The mass loss between 420 and 460 °C was presumably due to the loss of PAM moieties.[20] The first weight losses of GO and PAM/GO below 100 °C were estimated to be 7.98% and 12.63%, respectively. The second weight losses of GO and PAM/GO at 100–800 °C were about 23.67% and 35.31%, respectively. Accordingly, the percentage of PAM grafted on GO was calculated to be 11.64%.

Fig. 2c shows the Raman spectra of GO and PAM/GO. The peak at ~1580 cm^{-1} (G band) is related to the vibration of sp^2 carbon atoms in the 2D hexagonal lattice, and the peak at ~1350 cm^{-1} (D band) corresponds to the vibrations of sp^3 carbon atoms of defects and disorders. Compared with GO, the ratio of the intensities (I_D/I_G) of the PAM/GO nanosheets is remarkably increased after the plasma treatment, which indicates that PAM/GO contains a lower percentage of the sp^2 domains and PAM was successfully grafted onto the GO surfaces.[21]

The potentiometric acid–base titrations of GO and PAM/GO are shown in Fig. 2d. The surface sites of GO and PAM/GO (SOH) are considered amphoteric. They are positively charged at low pH because of the protonation reaction (*i.e.*, SOH + H$^+$ ⇔ SOH$_2^+$), while they are negatively charged at high pH because of the deprotonation reaction (*i.e.*, SOH ⇔ SO$^-$ + H$^+$).[22] The titration curves were collected in 0.01 mol L^{-1} NaCl solution, and both GO and PAM/GO displayed nearly identical buffering capacities across the pH range studied. At pH < 5.35, the surfaces of GO are positively charged, while at pH > 5.35, the surfaces of GO are negatively charged. However, at pH < 4.81, the surfaces of PAM/GO are positively charged, and at pH > 4.81 the surfaces of PAM/GO are negatively charged. After the grafting of PAM onto the surfaces of GO, the point of zero charge (pH$_{pzc}$) decreases from 5.35 (for GO) to 4.81 (for PAM/GO). This subtle change should be attributed to the low pK_a value of PAM, due to the –NH$_2^+$– and ═NH$^+$– groups.[23]

Fig. 2e shows the XRD patterns of natural graphite, GO and PAM/GO. It is well known that natural graphite has a strong diffraction peak at 26.21°, which does not appear in the XRD pattern of GO, indicating a complete oxidation of graphite. In addition, although GO itself shows a diffraction peak at 10.11°, PAM/GO does not present this peak, which may imply that the GO nanosheets are individually dispersed in the PAM/GO without multilayer GO stacks in the composites.[24] The DSC curves of GO and PAM/GO are shown in Fig. 2f. The thermogram of GO shows one strong exothermic peak at 175 °C, which is caused by the decomposition of organic groups in the GO sheets. For PAM/GO, the exothermic peak at 328 °C is caused by the decrease in the amount of labile functional groups.[25] The DSC curve of PAM/GO is quite different from that of PAM, which also suggests that PAM is not physically mixed with GO.[25a]

From the characterization results, one can deduce that PAM is chemically grafted on the GO surfaces. During the plasma-induced polymerization process, PAM and GO are activated by photons, electrons, or alpha particles, which are produced by exposure to the plasma. The activated PAM and GO form strong chemical bonds, thereby resulting in the grafting of PAM on GO.[25b,c]

Effect of contact time on radionuclide sorption

Fig. 3a shows that radionuclide sorption on PAM/GO is influenced by contact time. The amount of adsorbed radionuclides is enhanced with increasing contact time. The radionuclide sorption increases quickly in the initial 2 h of contact time, and then increases more slowly until the sorption process achieves equilibrium after 6 h. At the initial stages, many vacant surface sites are available for sorption. However, at later stages, the remaining vacant surface sites are difficult to occupy due to the repulsive forces between the sorbate molecules. Moreover, PAM/GO becomes nearly saturated with radionuclides at later stages, and the diffusion of radionuclides decreases as time passes.[26] In general, the sorption process is very rapid and 6 h is enough to achieve sorption equilibrium. The shaking time was fixed to 24 h in the following experiments to ensure that the removal process could achieve complete equilibrium. Two kinetic models, a pseudo-first-order ($\ln(Q_m - Q_1) = \ln Q_m - k't$) and a pseudo-second-order ($t/Q_1 = 1/(k''Q_m^2) + t/Q_m$) model, were applied to study the possible mechanism of the removal process.[27] Herein, Q_t and Q_m refer to the adsorbability of the radionuclides (mmol g^{-1}) at time t (h) and equilibrium adsorption ability obtained from the model, respectively. k' (1/h) and k'' (g mmol^{-1} h^{-1}) are the adsorption rate constants. The kinetic parameters obtained from both models are listed in Table 1. The pseudo-second-order model fits better than the

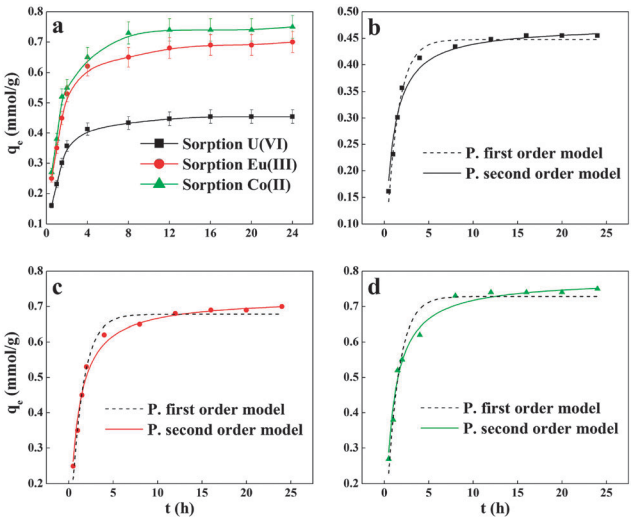

Fig. 3 Effect of contact time on the radionuclide sorption on PAM/GO (a); comparison of the two kinetic models of U(VI) (b), Eu(III) (c) and Co(II) (d) adsorption on PAM/GO, pH = 5.0 ± 0.1, T = 295 K, m/V = 0.2 g L^{-1}, $C_{initial}$ = 0.2 mmol L^{-1}, I = 0.01 mol L^{-1} NaCl.

Table 1 Parameters obtained from different kinetic models[a]

Model	Parameters	U(VI)	Eu(III)	Co(II)
Pseudo first order	k' (1 h)	0.766	0.753	0.759
	Q_{mc} (mmol g^{-1})	0.461	0.679	0.783
	R^2	0.99	0.984	0.966
Pseudo second order	k'' (g mmol^{-1} h^{-1})	0.921	0.788	0.756
	Q_{mc} (mmol g^{-1})	0.487	0.709	0.772
	R^2	0.999	0.999	0.998
	Q_{me} (mmol g^{-1})	0.492	0.698	0.771

[a] Q_{mc} is the adsorption capacity at equilibrium calculated by different models, Q_{me} is the experimental value.

pseudo-first-order model (Fig. 3) with the calculated maximum values (Q_{mc}) closer to the experimental ones (Q_{me}), highlighting the chemisorption-controlled mechanism.[28]

Effect of initial pH

The study of the effect of pH on radionuclide sorption on GO or PAM/GO nanosheets was carried out in the pH range of 2.0–11.0. Fig. 4 shows that radionuclide sorption onto the sorbent increases rapidly as pH increases in the pH range of 2.0–7.0. At pH > 7.0, the adsorption percentage of radionuclides on the sorbent decreases with increasing pH values. This effect can be attributed to the electrostatic attraction between the radionuclide species and the surface charges of PAM/GO, which are affected by the solution pH. Moreover, protonation–deprotonation reactions of functional groups could promote or suppress radionuclide sorption. From the potentiometric acid–base titrations (Fig. 2d), the surface of PAM/GO is found to be positively charged at pH < 4.81. Meanwhile, the dominant U(VI) species is UO_2^{2+} at pH < 5,[29] therefore, the electrostatic repulsion between PAM/GO and UO_2^{2+} leads to the low sorption of U(VI) onto PAM/GO. As pH increases, the functional groups on the surface of PAM/GO gradually become negatively charged. This increases the interaction between PAM/GO

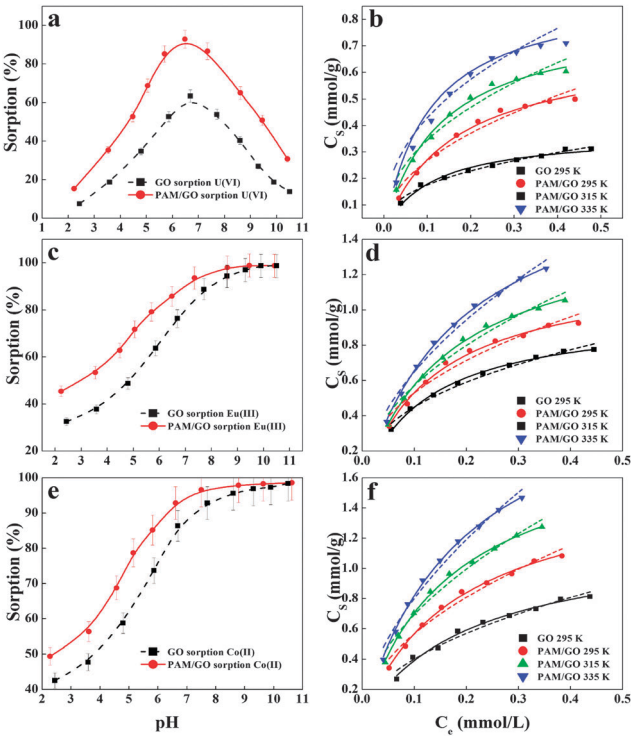

Fig. 4 Effect of pH on U(VI) (a), Eu(III) (c) and Co(II) (e) sorption to GO and PAM/GO, m/V = 0.2 g L^{-1}, I = 0.01 mol L^{-1} NaCl, $C_{initial}$ = 0.2 mmol L^{-1}; sorption isotherms of U(VI) (b), Eu(III) (d) and Co(II) (f) on GO and PAM/GO; the solid lines stand for the Langmuir model and the dashed lines stand for the Freundlich model, pH = 5.0 ± 0.1, m/V = 0.2 g L^{-1}, I = 0.01 mol L^{-1} NaCl.

and $(UO_2)_3(OH)_5^+/UO_2(OH)^+$, which are the dominant species of U(VI) between pH 5.0 and 7.0 (Fig. S2, ESI†). At pH > 7.0, the surface charges of the sorbents become more negative and $UO_2(OH)_3^-$ is the main species. The repulsion between $UO_2(OH)_3^-$ and the negatively charged surface results in the drop in U(VI) sorption. Eu(III) and Co(II) sorption onto PAM/GO nanosheets remains high when the pH is higher than 7.0, which can be attributed to surface complexation and precipitation (Fig. S3 and S4, ESI†).[5c,12b]

Sorption isotherms

Radioactive wastewater has a low pH value; hence, we estimated radionuclide sorption isotherms of PAM/GO at a pH of 5.0 (Fig. 4). As the radionuclide concentration increases, the amount of radionuclides adsorbed on PAM/GO firstly increases quickly and then arrives at a plateau. Fig. 4b, d and f show that the sorption isotherms increase with increasing temperature. This means that higher temperatures are more conducive to radionuclide sorption on PAM/GO. To further understand the sorption performance of PAM/GO, the experimental data were simulated by the Langmuir ($C_s = b \times C_{s\,max} - C_e/(1 + b \times C_e)$) and Freundlich ($C_s = K_F C_e^n$) models (where C_s is the amount of radionuclides adsorbed on PAM/GO (mmol g^{-1}), $C_{s\,max}$ is the maximum amount of radionuclides adsorbed on PAM/GO (mmol g^{-1}) at complete monolayer coverage, b (L mmol^{-1}) is the Langmuir constant that relates to the sorption heat, K_F (mmol^{1-n} L^n g^{-1}) represents the sorption capacity

Table 2 Parameters for the Langmuir and Freundlich models

		Langmuir model			Freundlich model		
Sorbent	T (K)	$C_{s\,max}$ (mmol g^{-1})	b (L mmol^{-1})	R^2	K_F (mmol^{1-n} L^n g^{-1})	n	R^2
U(VI)							
GO	295	0.373	9.176	0.978	0.424	0.384	0.986
	295	0.698	6.376	0.994	0.788	0.469	0.959
PAM/GO	315	0.809	7.831	0.994	0.954	0.441	0.960
	335	0.917	9.595	0.993	0.418	0.488	0.961
Eu(III)							
GO	295	0.986	8.307	0.996	1.109	0.393	0.984
	295	1.245	7.419	0.994	1.423	0.429	0.961
PAM/GO	315	1.506	6.139	0.998	1.735	0.483	0.975
	335	1.917	5.192	0.998	2.253	0.541	0.982
Co(II)							
GO	295	1.208	4.776	0.991	1.283	0.506	0.974
	295	1.621	5.366	0.997	1.849	0.514	0.976
PAM/GO	315	1.911	5.845	0.998	2.309	0.523	0.980
	335	2.401	5.176	0.998	3.001	0.574	0.983

when the equilibrium concentration of radionuclides is equal to 1, and n represents the degree of dependence of the sorption on the equilibrium concentration).

From Table 2 and Fig. 4, one can see that the Langmuir model fits the experimental data better than the Freundlich model. At pH = 5.0 ± 0.1 and T = 295 K, the $C_{s\,max}$ values of U(VI), Eu(III) and Co(II) on PAM/GO are 0.698, 1.245 and 1.621 mmol g^{-1} respectively, which are far higher than the values for those radionuclides on GO and other adsorbents under similar experimental conditions (Table S4, ESI†). One can see that the PAM/GO nanosheets present a high adsorption capability for radionuclides. As mentioned above, the modified PAM on the GO surface could enhance the sorption of radionuclides because of the stronger complexation between nitrogen- and/or oxygen-containing functional groups and radionuclides. The PAM significantly increases the surface area of PAM/GO, which can provide more active sites and functional groups for radionuclide uptake. The results indicate that PAM/GO is potentially able to be used as a highly efficient material in the treatment of radioactive wastewater.

Thermodynamic analysis

The sorption of radionuclides increases with increasing reaction temperature. The highest sorption isotherm is obtained at T = 335 K while the lowest sorption isotherm is obtained at T = 295 K, which illustrates that the sorption of radionuclides on PAM/GO is promoted at higher temperatures. The thermodynamic parameters (ΔG^0, ΔS^0 and ΔH^0) were calculated from the temperature-dependent sorption isotherms. The value of free energy change was derived from the equation $\Delta G^0 = -RT \ln K^0$ (K^0 is the constant of sorption equilibrium). The values of $\ln K^0$ stand for the sorption abilities of PAM/GO toward radionuclides. The standard enthalpy change (ΔH^0) and the standard entropy change (ΔS^0) were calculated from the equation $\Delta G^0 = \Delta H^0 - T\Delta S^0$; R (8.314 J mol^{-1} K^{-1}) is the constant of ideal gas and T (K) is the temperature. The values calculated from the thermodynamic equations are listed in Table 3. The positive ΔH^0 value and negative ΔG^0 value reveal that the sorption reaction is a spontaneous and endothermic process. This is in line with the fact that the sorption increases as the reaction temperature increases. A probable explanation for the positive enthalpy is the complete dissolution of radionuclides in water; the hydration sheaths of the radionuclides are supposed to be destroyed before the ions are adsorbed on PAM/GO, and the energy required for this dehydration process exceeds the energy released during the attachment of cations to the solid surface.[30]

Table 3 Thermodynamic parameters for radionuclide sorption on PAM/GO

Adsorbate	T (K)	ΔG^0 (kJ mol^{-1})	ΔS^0 (J mol^{-1}K^{-1})	ΔH^0 (kJ mol^{-1})
U(VI)	295	−16.63	56.37	13.52
	315	−17.76		
	335	−18.88		
Eu(III)	295	−8.71	29.53	3.96
	315	−9.30		
	335	−9.89		
Co(II)	295	−13.19	44.70	82.93
	315	−14.08		
	335	−14.98		

Effect of ionic strength

The effect of ionic strength on the adsorption of radionuclides onto PAM/GO was studied under different NaCl concentrations (Fig. 5a). It can be seen that the sorption percentage decreases with increasing NaCl concentration. The adsorption percentages of radionuclides on PAM/GO decrease by more than 20% as the concentration of NaCl in solution increases from 0.005 mmol L^{-1} to 0.05 mol L^{-1}. This phenomenon has also been found in other studies.[31] The ionic strength plays a key role in controlling electrostatic interactions. Hence, these interactions, attractive or repulsive, are decreased with increasing NaCl concentration. High ionic strength will cause a screening effect.[32] The increase in ionic strength would inhibit the electrostatic interactions between the radionuclides and the

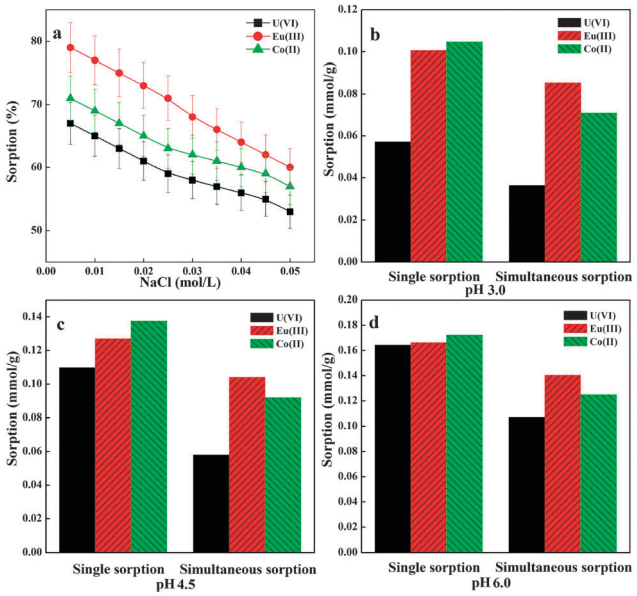

Fig. 5 Effect of ionic strength on radionuclide sorption onto PAM/GO (a), pH = 5.0 ± 0.1, T = 295 K, m/V = 0.2 g L^{-1}, $C_{initial}$ = 0.2 mmol L^{-1}; single and simultaneous sorption of radionuclides on PAM/GO at three pH values (b–d), T = 295 K, m/V = 0.2 g L^{-1}.

charged amino groups and deprotonated carboxyl groups of PAM/GO.[33] When radionuclides are present in a solution of high ionic strength, their activities are heavily decreased, which finally inhibits their movement to the surface of PAM/GO. Moreover, high ionic strength can also decrease the electrostatic repulsion between PAM/GO, which results in aggregation and lower adsorption ability of PAM/GO. The ionic strength dependence of the radionuclide sorption indicates a surface complexation mechanism.[33]

Simultaneous sorption

The simultaneous sorption of U(VI), Eu(III) and Co(II) from water by PAM/GO, which should contribute to the treatment of radionuclide pollution, was investigated. The experiment was carried out at three pH values (*i.e.*, pH 3.0, 4.5 and 6.0) in a 1 L beaker, which contained 0.2 g L^{-1} PAM/GO and 0.2 mmol L^{-1} radionuclides (U(VI), Eu(III) and Co(II)), respectively. As shown in Fig. 5b–d, compared to single sorption, the sorption percentages of PAM/GO towards U(VI), Eu(III) and Co(II) decrease by about 10–30% at the three pH values. From the values listed in Table 4, one can see that the simultaneous sorption of radionuclides leads to an increase in the total uptake of radionuclides and a decrease in the single sorption of each radionuclide. Significant competitive interactions between different species in solution may exist. The adsorbability of PAM/GO for different radionuclides should be affected by a series of factors, including ionic size, ionic charge, functional groups and surface properties.[34] According to previous studies, the ionic radius of Eu(III) is 0.113 nm,[35] and the ionic radius of Co(II) is 0.082 nm;[36] while the dumb-bell shaped UO_2^{2+}, which is the dominant U(VI) species at pH < 5.0,[37] has a linear structure with an overall length of 0.36 nm.[38] A higher valence ion is rather more easily adsorbed on PAM/GO; therefore, Eu(III) has the highest affinity to PAM/GO surface. The radius of Co(II) is smaller than that of UO_2^{2+}, thus leading to higher adsorbability. So the relative affinity of the PAM/GO surface for the radionuclides is in the order Eu(III) > Co(II) > U(VI). Similar results were also reported for Cd(II) and Co(II) sorption on the exopolysaccharide produced by *Chryseomonas luteola*.[39] The results herein manifest that the use of PAM/GO for radionuclide removal is highly efficient and versatile.

Table 4 Comparison of single sorption and simultaneous sorption of radionuclides onto PAM/GO (mmol g^{-1})

	Single sorption			Simultaneous sorption		
pH	U(VI)	Eu(III)	Co(II)	U(VI)	Eu(III)	Co(II)
3.0	0.0571	0.1007	0.1047	0.0365	0.0854	0.0710
4.5	0.1097	0.1271	0.1375	0.0579	0.1041	0.0919
6.0	0.1644	0.1664	0.1723	0.1069	0.1403	0.1249

XPS analysis

In order to study the sorption of radionuclides on PAM/GO at a molecular level, the interaction of radionuclides with PAM/GO was studied by using X-ray photoelectric spectroscopy (XPS). As shown in Fig. 6a, peaks are seen for the expected components of PAM/GO, and the characteristic peaks of radionuclides appear, which suggests that a significant amount of radionuclides is adsorbed onto PAM/GO. The peaks at 392.98 and 382.28 eV are the characteristic doublets of U $4f_{5/2}$ and U $4f_{7/2}$ from uranium with a splitting of about 10.7 eV (Fig. 6b).[40] The U 4f spectrum is resolved into two peaks: the peak at 382.5 eV corresponds to the free uranyl adsorbed on PAM/GO, and the peak at 381.1 eV is attributed to a covalent bond of amido-U(VI).[41] The peaks at 1134.8 and 1164.2 eV are the characteristic doublets of Eu $3d_{5/2}$ and Eu $3d_{3/2}$ from europium (Fig. 6c).

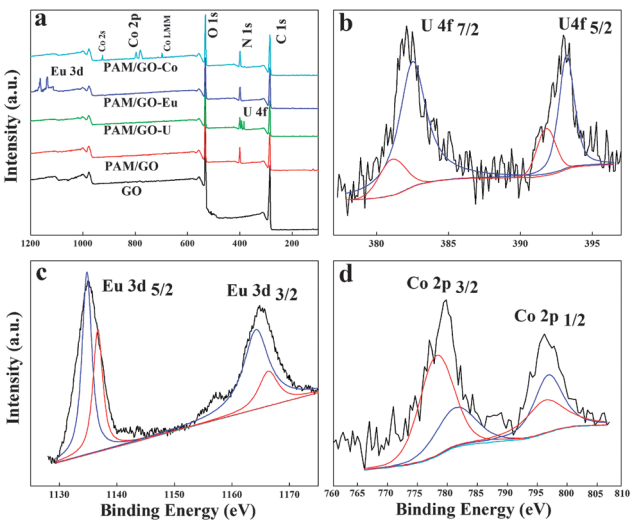

Fig. 6 XPS survey scans and high resolution spectra of PAM/GO and PAM/GO-radionuclides, total survey scans (a); U 4f spectrum (b); Eu 3d spectrum (c); Co 2p spectrum (d), pH = 5.0 ± 0.1, T = 295 K, m/V = 0.2 g L^{-1}, $C_{initial}$ = 0.2 mmol L^{-1}, I = 0.01 mol L^{-1} NaCl.

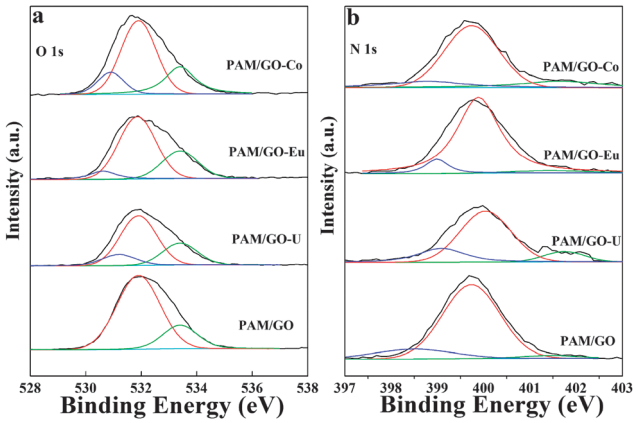

Fig. 7 High-resolution XPS spectra of PAM/GO-radionuclides, O 1s spectra (a), N 1s spectra (b), pH = 5.0 ± 0.1, T = 295 K, m/V = 0.2 g L^{-1}, $C_{initial}$ = 0.2 mmol L^{-1}, I = 0.01 mol L^{-1} NaCl.

The Eu 3d spectrum is resolved into two peaks, which represent two types of species that could form complexes with nitrogen- and oxygen-containing functional groups.[11a] The Co 2p XPS spectrum shows two major peaks with binding energies at 781.08 and 796.08 eV, corresponding to Co $2p_{3/2}$ and Co $2p_{1/2}$, respectively, with a spin-energy separation of 15 eV (Fig. 6d).[42] The Co 2p spectrum is resolved into two peaks: the peak at 780.45 eV corresponds to a covalent bond of oxygen-Co(II), and the peak at 782.16 eV is attributed to a covalent bond of amido-Co(II).[43]

The O 1s peaks of PAM/GO and PAM/GO-radionuclides are shown in Fig. 7a. The binding energies at 531.2, 531.8 and 533.4 eV can be assigned to bridging –OH, C═O, and alcoholic C–O, respectively.[44] Compared to PAM/GO, the bridging –OH is observable and the relative intensities of the C═O and alcoholic C–O peaks of PAM/GO-radionuclides decrease. The great variation of O 1s before and after radionuclide sorption indicates that radionuclides can form strong complexes with oxygen-containing functional groups. Fig. 7b shows the N 1s spectra of PAM/GO before and after radionuclide sorption. The N 1s spectrum is resolved into three individual component peaks at 398.79, 399.74 and 401.64 eV.[41c] The peak at 399.74 eV is due to the nitrogen atoms in PAM, the peak at 401.64 eV is attributed to the complexes of $-NH_2$ and cations,[45] and the peak at 398.79 eV is ascribed to the formation of covalent amido-cation bonds, in which the cations share electrons with the nitrogen atom of the O═C–NH_2 group.[41c]

Before radionuclide sorption, a dominant peak appears at 399.79 eV; additionally, two very small peaks are found at 401.64 eV and 398.79 eV. The atomic contents of the radionuclides on PAM/GO are in accordance with the decrease in the percentages of C, N and O observed after radionuclide sorption compared to PAM/GO before radionuclide sorption (Table S5, ESI†). Moreover, the peak fitting results of the U 4f, Eu 3d, Co 2p, O 1s and N 1s before and after radionuclide sorption on PAM/GO are listed in Table S6 (ESI†). The sorption of radionuclides on PAM/GO leads to a decrease in the percentages of N 1s and O 1s peaks. Based on analysis of the XPS spectra, the high adsorbability of PAM/GO nanosheets is largely due to a large number of nitrogen- and oxygen-containing functional groups, which can easily form strong complexes with radionuclides on the PAM/GO surface.

Conclusions

To conclude, we synthesized highly dispersed PAM/GO nanosheets by a simple, green and low-cost plasma approach. Analysis of the results of SEM, TEM, FT-IR, TGA, Raman spectroscopy and potentiometric acid–base titrations indicated that PAM was successfully modified onto the surface of GO. The equilibrium sorption data were well fitted by the Langmuir sorption isotherms, and PAM/GO exhibited high sorption capacity for radionuclides. The thermodynamic parameters indicated that the interaction of radionuclides with PAM/GO was an endothermic and spontaneous process. Simultaneous sorption results indicated that the PAM/GO could adsorb the radionuclides simultaneously, and the simultaneous sorption capacity was higher than that of single radionuclide sorption. On the basis of the XPS analysis, the sorption of radionuclides was mainly due to nitrogen- and oxygen-containing functional groups on PAM/GO surfaces, which could form strong complexes with radionuclides. These results show that PAM/GO is a very suitable material for radioactive wastewater treatment and that the plasma approach is promising for the future synthesis of these kinds of nanomaterials.

Acknowledgements

Financial support from National Natural Science Foundation of China (11305218, 21225730, 91326202), the Science Foundation of Institute of Plasma Physics, Chinese Academy of Sciences (DSJJ-13-YY01) and the Jiangsu Provincial Key Laboratory of Radiation Medicine and Protection and the Priority Academic Program Development of Jiangsu Higher Education Institutions are acknowledged.

References

1 (*a*) L. M. Camacho, S. G. Deng and R. R. Parra, *J. Hazard. Mater.*, 2010, **175**, 393; (*b*) T. B. Scott, G. C. Allen, P. J. Heard and M. G. Randell, *Geochim. Cosmochim. Acta*, 2005, **69**, 5639.

2 (*a*) J. M. Monsallier, W. Schussler, G. Buckau, T. Rabung and J. Kim, *Anal. Chem.*, 2003, **75**, 3168; (*b*) B. Gu, Y. K. Ku and P. M. Jardine, *Environ. Sci. Technol.*, 2004, **38**, 3184; (*c*) X. K. Wang, C. L. Chen, J. Z. Du, X. L. Tan, D. Xu and S. M. Yu, *Environ. Sci. Technol.*, 2005, **39**, 7084.

3 (*a*) W. Um, S. Mattigod, R. J. Serne, G. E. Fryxell, D. H. Kim and L. D. Troyer, *Water Res.*, 2007, **41**, 3217; (*b*) S. Kasap, S. Piskin and H. Tel, *Radiochim. Acta*, 2012, **100**, 925; (*c*) Y. B. Sun, S. T. Yang, G. D. Sheng, Z. Q. Guo, X. L. Tan, J. Z. Xu and X. K. Wang, *Sep. Purif. Technol.*, 2011, **83**, 196; (*d*) X. X. Wang, S. W. Zhang, J. X. Li, J. Z. Xu and X. K. Wang, *Inorg. Chem. Front.*, 2014, **1**, 641.

4 (*a*) X. K. Wang, C. L. Chen, W. P. Hu, A. P. Ding, D. Xu and X. Zhou, *Environ. Sci. Technol.*, 2005, **39**, 2856; (*b*) J. Hu, D. Shao, C. Chen, G. Sheng, J. Li, X. Wang and M. Nagatsu, *J. Phys. Chem. B*, 2010, **114**, 6779; (*c*) C. L. Chen, X. K. Wang and M. Nagatsu, *Environ. Sci. Technol.*, 2009, **43**, 2362; (*d*) D. D. Shao, Z. Q. Jiang, X. K. Wang, J. X. Li and Y. D. Meng, *J. Phys. Chem. B*, 2009, **113**, 860.

5 (*a*) G. X. Zhao, J. X. Li, X. M. Ren, C. L. Chen and X. K. Wang, *Environ. Sci. Technol.*, 2011, **45**, 10454; (*b*) G. X. Zhao, T. Wen, X. T. Yang, S. B. Yang and X. K. Wang, *Dalton Trans.*, 2012, **41**, 6182; (*c*) Y. B. Sun, Q. Wang, C. L. Chen, X. L. Tan and X. K. Wang, *Environ. Sci. Technol.*, 2012, **46**, 6020.

6 (*a*) Y. Zhu, S. Murali, W. Cai, X. Li, J. W. Suk, J. R. Potts and R. S. Ruoff, *Adv. Mater.*, 2010, **22**, 3906; (*b*) H. K. He and C. Gao, *Sci. China: Chem.*, 2011, **54**, 397.

7 A. Y. Romanchuk, A. S. Slesarev, S. N. Kalmykov, D. V. Kosynkin and J. M. Tour, *Phys. Chem. Chem. Phys.*, 2013, **15**, 2321.

8 D. R. Dreyer, S. Park, C. W. Bielawski and R. S. Ruoff, *Chem. Soc. Rev.*, 2010, **39**, 228.

9 (*a*) S. Park, K. S. Lee, G. Bozoklu, W. Cai, S. T. Nguyen and R. S. Ruoff, *ACS Nano*, 2008, **2**, 572; (*b*) R. Hu, D. D. Shao and X. K. Wang, *Polym. Chem.*, 2014, **5**, 6207.

10 (*a*) Y. X. Xu, Q. Wu, Y. Q. Sun, H. Bai and G. Q. Shi, *ACS Nano*, 2010, **4**, 7358; (*b*) D. S. Xiang, A. H. Zhang, M. Luo, X. H. Ji and Z. K. He, *Sci. China: Chem.*, 2013, **56**, 380.

11 (*a*) Y. B. Sun, D. D. Shao, C. L. Chen, S. B. Yang and X. K. Wang, *Environ. Sci. Technol.*, 2013, **47**, 9904; (*b*) Y. Q. Chen, L. B. Chen, H. Bai and L. Li, *J. Mater. Chem. A*, 2013, **1**, 1992.

12 (*a*) Y. G. Zhao, J. X. Li, S. W. Zhang, H. Chen and D. D. Shao, *RSC Adv.*, 2013, **3**, 18952; (*b*) W. C. Song, J. Hu, Y. Zhao, D. D. Shao and J. X. Li, *RSC Adv.*, 2013, **3**, 9514; (*c*) C. J. Madadrang, H. Y. Kim, G. Gao, N. Wang, J. Zhu, H. Feng and S. Hou, *ACS Appl. Mater. Interfaces*, 2012, **4**, 1186; (*d*) G. X. Zhao, L. Jiang, Y. D. He, J. X. Li, H. K. Dong, X. K. Wang and W. P. Hu, *Adv. Mater.*, 2011, **23**, 3959.

13 (*a*) U. Ulusoy, S. Şimşek and Ö. Ceyhan, *Adsorption*, 2003, **9**, 165; (*b*) U. Ulusoy and R. Akkaya, *J. Hazard. Mater.*, 2009, **163**, 98; (*c*) I. G. Shibi and T. S. Anirudhan, *Chemosphere*, 2005, **58**, 1117; (*d*) R. Coşkun, C. Soykan and M. Saçak, *Sep. Purif. Technol.*, 2006, **49**, 107; (*e*) S. B. Yang, J. Hu, C. L. Chen, D. D. Shao and X. K. Wang, *Environ. Sci. Technol.*, 2011, **45**, 3621; (*f*) H. B. Sonmez, B. F. Senkal and N. Bicak, *J. Polym. Sci., Part B: Polym. Phys.*, 2002, **40**, 3068; (*g*) I. G. Shibi and T. S. Anirudhan, *Ind. Eng. Chem. Res.*, 2002, **41**, 5341; (*h*) H. Sigel and R. B. Martin, *Chem. Rev.*, 1982, **82**, 385; (*i*) G. N. Manju, K. A. Krishnan, V. P. Vinod and T. S. Anirudhan, *J. Hazard. Mater.*, 2002, **91**, 221.

14 (*a*) Q. Wang, M. M. Song, C. L. Chen, Y. Wei, X. Zuo and X. K. Wang, *Appl. Phys. Lett.*, 2012, **101**, 033103; (*b*) Q. Wang, M. M. Song, C. L. Chen, W. P. Hu and X. K. Wang, *ChemPlusChem*, 2012, **77**, 432; (*c*) Q. Wang, X. K. Wang, Z. F. Chai and W. P. Hu, *Chem. Soc. Rev.*, 2013, **42**, 8821.

15 M. Hirata, T. Gotou, S. Horiuchi, M. Fujiwara and M. Ohba, *Carbon*, 2004, **42**, 2929.

16 (*a*) Q. Zhou, Z. B. Zhao, Y. S. Chen, H. Hu and J. S. Qiu, *J. Mater. Chem.*, 2012, **22**, 6061; (*b*) W. Y. Xu, X. Z. Wang, Q. Zhou, B. Meng, J. T. Zhao, J. S. Qiu and Y. Gogotsi, *J. Mater. Chem.*, 2012, **22**, 14363.

17 N. A. Kumar, H. J. Choi, Y. R. Shin, D. W. Chang, L. Dai and J. B. Baek, *ACS Nano*, 2012, **6**, 1715.

18 (*a*) G. X. Zhao, H. X. Zhang, Q. H. Fan, X. M. Ren, J. X. Li, Y. X. Chen and X. K. Wang, *J. Hazard. Mater.*, 2010, **173**, 661; (*b*) H. Kaşgöz, S. Özgümüş and M. Orbay, *Polymer*, 2003, **44**, 1785.

19 C. B. Li, X. R. Wang, Y. Liu, W. Wang, J. Wynn and J. P. Gao, *J. Nanopart. Res.*, 2012, **14**, 1.

20 (*a*) S. Sun and P. Wu, *J. Mater. Chem.*, 2011, **21**, 4095; (*b*) J. F. Shen, B. Yan, T. Li, Y. Long, N. Li and M. X. Ye, *Composites, Part A*, 2012, **43**, 1476.

21 S. Stankovich, D. A. Dikin, R. D. Piner, K. A. Kohlhaas, A. Kleinhammes, Y. Jia, Y. Wu, S. T. Nguyen and R. S. Ruoff, *Carbon*, 2007, **45**, 1558.

22 C. L. Chen, J. Hu, D. Xu, X. L. Tan, Y. D. Meng and X. K. Wang, *J. Colloid Interface Sci.*, 2008, **323**, 33.

23 C. Menardo, M. Nechtschein, A. Rousseau and J. P. Travers, *Synth. Met.*, 1988, **25**, 311.

24 R. Liu, S. Liang, X. Z. Tang, D. Yan, X. Li and Z. Z. Yu, *J. Mater. Chem.*, 2012, **22**, 14160.

25 (*a*) C. S. Wang, Q. C. Jin, Y. T. Wang, H. Y. Yin, H. F. Xie and R. S. Cheng, *Mater. Lett.*, 2012, **68**, 280; (*b*) D. D. Shao, J. Hu and X. K. Wang, *Plasma Processes Polym.*, 2010, **7**, 977; (*c*) D. D. Shao, Z. Q. Jiang and X. K. Wang, *Plasma Processes Polym.*, 2010, **7**, 552.

26 K. G. Bhattacharyya and S. S. Gupta, *Chem. Eng. J.*, 2008, **136**, 1.

27 (*a*) Q. Wang, J. X. Li, Y. Song and X. K. Wang, *Chem. – Asian J.*, 2013, **8**, 225; (*b*) M. Alkan, M. Doğan, Y. Turhan, Ö. Demirbaş and P. Turan, *Chem. Eng. J.*, 2008, **139**, 213.

28 A. Chen, C. Yang and C. Chen, *J. Hazard. Mater.*, 2009, **163**, 1068.

29 S. T. Yang, P. F. Zong, J. Hu, G. D. Sheng, Q. Wang and X. K. Wang, *Chem. Eng. J.*, 2013, **214**, 376.

30 (*a*) G. D. Sheng, J. X. Li, D. D. Shao, J. Hu, C. L. Chen, Y. X. Chen and X. K. Wang, *J. Hazard. Mater.*, 2010, **178**, 333; (*b*) G. D. Sheng, H. P. Dong, R. P. Shen and Y. M. Li, *Chem. Eng. J.*, 2013, **217**, 486.

31 L. L. Ji, W. Chen, J. Bi, S. R. Zheng, Z. Y. Xu, D. Q. Zhu and P. J. Alvarez, *Environ. Toxicol. Chem.*, 2010, **29**, 2713.

32 C. Moreno-Castilla, M. A. Alvarez-Merino, M. V. López-Ramón and J. Rivera-Utrilla, *Langmuir*, 2004, **20**, 8142.

33 Y. Gao, Y. Li, L. Zhang, H. Huang, J. J. Hu, S. M. Shah and X. G. Su, *J. Colloid Interface Sci.*, 2012, **368**, 540.

34 C. Mahamadi and T. Nharingo, *Bioresour. Technol.*, 2010, **101**, 859.

35 Y. H. Zhou, J. Lin, S. B. Wang and H. Zhang, *Opt. Mater.*, 2002, **20**, 13.

36 D. M. Hemeda, A. Al-Sharif and O. M. Hemeda, *J. Magn. Magn. Mater.*, 2007, **315**, L1.

37 W. C. Song, M. C. Liu, R. Hu, X. L. Tan and J. X. Li, *Chem. Eng. J.*, 2014, **246**, 268.
38 K. Bohinc, J. Rescis, J. F. Dufreche and L. Lue, *J. Phys. Chem. B*, 2013, **117**, 10846.
39 G. Ozdemir, N. Ceyhan and E. Manav, *Bioresour. Technol.*, 2005, **96**, 1677.
40 (*a*) T. S. Anirudhan and S. Rijith, *J. Environ. Radioact.*, 2012, **106**, 8; (*b*) D. B. Beach, K. D. bomben, N. M. Edelstein, D. C. Eisenberg, W. L. Jolly, R. Shinomoto and A. Streitwieser Jr, *Inorg. Chem.*, 1986, **25**, 1735.
41 (*a*) H. J. Yan, J. W. Bai, X. Chen, J. Wang, H. S. Zhang, Q. Liu, M. L. Zhang and L. H. Liu, *RSC Adv.*, 2013, **3**, 23278; (*b*) E. Ordonez-Regil, R. Drot, E. Simoni and J. J. Ehrhardt, *Langmuir*, 2002, **18**, 7977; (*c*) Y. J. Zhao, Y. Chen, M. S. Li, S. Y. Zhou, A. L. Xue and W. H. Xing, *J. Hazard. Mater.*, 2009, **171**, 640.
42 (*a*) J. Yan, T. Wei, W. M. Qiao, B. Shao, Q. K. Zhao, L. J. Zhang and Z. J. Fan, *Electrochim. Acta*, 2010, **55**, 6973; (*b*) S. L. Xiong, C. Z. Yuan, M. F. Zhang, B. J. Xi and Y. T. Qian, *Chem. – Eur. J.*, 2009, **15**, 5320.
43 M. H. Koppelman and J. G. Dillard, *J. Colloid Interface Sci.*, 1978, **66**, 345.
44 (*a*) S. B. Deng and Y. P. Ting, *Water Res.*, 2005, **39**, 2167; (*b*) H. Wang, A. Zhou, F. Peng, H. Yu and J. Yang, *J. Colloid Interface Sci.*, 2007, **316**, 277; (*c*) X. L. Tan, Q. H. Fan, X. K. Wang and B. Grambow, *Environ. Sci. Technol.*, 2009, **43**, 3115.
45 L. Jin and R. Bai, *Langmuir*, 2002, **18**, 9765.

